Vol. 48, No. 3 (2026) 645-658, DOI: 10.24874/ti.2206.05.26.06

Tribology in Industry

www.tribology.rs

RESEARCH

Friction-Induced Effects on Band Saw Blade Lateral Dynamics: A PDE-Based Tribological Model

Damjan Stanojevic[a], Dragan Dzunic[b], Vladimir M. Markovic[c,*]

[a]*Academy of Technical and Educational Vocational Studies Niš, Department of Vranje, Serbia,*
[b]*Faculty of Engineering, University of Kragujevac, Serbia,*
[c]*Department of Physics, Faculty of Science, University of Kragujevac, Serbia.*

Keywords:

Band saw dynamics
Friction coefficient
Cutting force modeling
Blade deflection
Tribological effects

* Corresponding author:

Vladimir M. Markovic
E-mail: vmarkovic@kg.ac.rs

Received: 4 May 2026
Revised: 16 June 2026
Accepted: 16 July 2026

A B S T R A C T

The lateral dynamics of a band saw blade during cutting is investigated using a distributed-parameter model that combines mechanical and tribological effects. The active blade span between two lateral guides is represented as a tensioned continuous system governed by a damped wave equation, while cutting is introduced through a localized feed-speed-dependent force. Friction is modeled by an effective Coulomb-type term $F_f = \mu F_N$, with a constant representative normal contact force. The governing equation is solved using an explicit finite-difference scheme. Simulations without friction show bounded oscillatory motion dominated by the harmonic component of the cutting force, whereas feed speed has only a minor influence. For $F_N = 200\ N$, the maximum displacement increases from $0.213\ mm$ at $\mu = 0$ to $1.036\ mm$ at $\mu = 0.6$, corresponding to an approximately five-fold increase. The dependence on μ is nearly linear, as expected from the adopted friction law. For a guide spacing of $L = 0.31\ m$, the predicted displacement well agrees with experimentally reported values for a comparable band-saw configuration. The results show that frictional conditions and guide spacing strongly influence lateral deflection and may therefore affect cutting accuracy. The model provides a transparent framework for parametric analysis, while machine-specific prediction requires experimentally calibrated contact parameters.

© 2026 Published by Faculty of Engineering

1. INTRODUCTION

Band sawing is one of the most important machining operations in primary wood processing, owing to its high productivity, narrow kerf width, and ability to continuously process large workpieces. Despite its industrial importance, maintaining stable cutting conditions and consistent surface quality remains a significant challenge. The quality of the sawn surface is strongly affected by the dynamic response of the saw blade, particularly by lateral deflection and vibration, which may lead to surface waviness, increased roughness, dimensional deviations, and material losses.

From a mechanical point of view, the band saw blade represents a slender, tensioned structural element operating under high speed and repeated tooth–workpiece interaction. Its lateral motion is governed by the combined influence of axial tension, inertia, damping, and localized cutting forces. Classical vibration theory provides a suitable basis for describing such flexible systems using string- or beam-type models, depending on the relative importance of axial tension and bending stiffness [1]. In the case of band saw blades operating under sufficiently high pretension, the tension-induced restoring force often dominates the bending contribution, making a tensioned-continuum approximation appropriate for first-order dynamic analysis [2,3].

In addition to structural dynamics, band sawing is inherently a tribological process. The cutting zone involves contact between the blade teeth, the lateral blade surfaces, and the workpiece material. During cutting, frictional interaction contributes to force generation, heat production, tool wear, energy consumption, and deterioration of surface quality. Therefore, the blade–wood interface should not be treated only as a source of mechanical loading, but also as a contact system in which friction and wear-related effects influence the dynamic behavior of the tool. This is particularly important for wood machining, where the coefficient of friction may depend on surface roughness, contact pressure, moisture content, fiber orientation, sliding direction, and tool condition [4,5].

Cutting forces in wood machining are commonly related to chip formation, feed speed, tool geometry, and workpiece properties. Increasing feed speed generally increases chip thickness and mechanical loading, which can amplify blade deflection and reduce cutting accuracy. Previous investigations have shown that cutting conditions and tool properties have a strong influence on sawing forces and surface quality [6-8]. Recent measurements performed for clear and knotty pine have further demonstrated that wood heterogeneity can produce substantial variations in cutting forces, confirming the importance of material-dependent dynamic excitation in wood sawing [9]. Orlowski et al. [7] emphasized that modern descriptions of wood sawing should account not only for cutting resistance but also for friction between the tool and the workpiece. This point is especially relevant for narrow-kerf sawing, where relatively small changes in lateral blade displacement may have significant effects on cutting precision.

Tool geometry and wear further strengthen the connection between tribology and blade dynamics. The elastic spring-back of wood after passage of the cutting edge can produce contact between the workpiece and the major or minor flank surfaces of the teeth, thereby increasing frictional forces and modifying the lateral loading of the blade. The magnitude of this interaction depends on tooth clearance angles, cutting direction, wood structure, and the available kerf clearance [10]. Worn or damaged cutting edges may additionally increase frictional resistance, alter force transmission, and intensify vibration. Recent investigations of coated cutting tools have shown that cutting-edge microgeometry, surface coatings, and wear mechanisms strongly influence friction, cutting stability, and tool durability in wood processing [11]. These findings support the development of models that connect cutting-force generation, frictional contact, and structural blade response.

Several modelling approaches have been applied to cutting processes and saw-blade dynamics, including analytical distributed-parameter models, lumped-parameter formulations, finite-element simulations, and more detailed machining-dynamics models [2,3,12,13]. High-fidelity numerical approaches can describe local structural and contact effects in considerable detail, but they generally require numerous material, geometric, and contact parameters. Reduced partial-differential-equation models offer a useful compromise between physical transparency and computational efficiency, particularly when the objective is to isolate the influence of selected operating and tribological parameters. More broadly, recent studies identify stick–slip, mode coupling, and friction–velocity effects as important mechanisms of friction-induced vibration, while experimental investigations of band-saw guides confirm that guide design and guide–blade interaction can strongly affect lateral vibration, blade alignment, wear, and the resulting surface quality [14,15].

Many existing models of band saw or saw-blade dynamics focus primarily on structural vibration and cutting-force excitation, while the frictional contribution at the tool–workpiece interface is often included only implicitly or neglected. However, for a tribological interpretation of sawing, the cutting force should be decomposed into a component associated with material separation and a component associated with frictional contact. Even if the normal contact force is not measured directly, it can be introduced through a Coulomb-type friction term $F_f = \mu F_N$, where the normal contact force F_N is represented by a constant value that reflects the lateral pressure between the blade and the workpiece. This enables systematic parametric analysis of the influence of friction on lateral blade deflection, without introducing artificial coupling between feed speed and normal load.

The present study develops a PDE-based dynamic model of band saw blade lateral deflection under variable feed conditions, extended by an effective frictional contact term. The blade is modeled as a tensioned continuous system subjected to localized excitation at the cutting zone. The cutting force depends on feed speed and includes a time-dependent perturbation, while the frictional contribution is introduced through a Coulomb-type term μF_N, where the normal contact force F_N is estimated from the lateral pressure exerted by the workpiece on the blade sides and is taken as constant for the purposes of this parametric study. This formulation allows direct comparison between a reference case without friction and tribological cases with nonzero friction coefficients.

The novelty of the present work does not lie in the use of the tensioned-string equation or the finite-difference method themselves, which are established modelling tools. Rather, it lies in the explicit integration of a localized, feed-dependent cutting-force model with an effective Coulomb-type lateral friction load within a guide-bounded active blade span. This formulation enables the mechanical and tribological contributions to the blade response to be separated and compared directly.

The specific contributions are: (i) formulation of the active blade segment between two lateral guides as the computational domain; (ii) incorporation of a localized cutting force containing both feed-dependent and harmonic components; (iii) introduction of an effective frictional load $F_f = \mu F_N$ acting at the cutting zone; (iv) direct parametric quantification of the influence of $\mu$and F_N on lateral blade displacement; and (v) literature-based comparison of the predicted displacement magnitude with an experimentally reported guide-bounded band-saw configuration. The resulting model is intended as a transparent reduced framework for assessing how cutting mechanics, frictional loading, and guide spacing jointly influence the lateral response of the blade.

2. METHODOLOGY

The dynamic behavior of a band saw blade during cutting is governed by the interaction between its structural properties and the forces generated in the cutting zone. Due to its slender geometry, high tensile loading, and continuous motion, the blade can be effectively modeled as a flexible, tensioned continuum. This approach is consistent with classical vibration theory, where similar systems are described either as strings or beams under axial tension [1,2,3].

2.1 Blade model, assumptions, and range of validity

In the present study, the blade is represented as a one-dimensional continuous system with lateral displacement $w(x,t)$, where x denotes the spatial coordinate along the blade and t is time. The analysis focuses on lateral deflection, which is the dominant mechanism affecting cutting accuracy and surface quality. The blade is assumed to be under constant axial tension, with uniform material and geometric properties. The deflections are considered small, allowing linearization of the governing equation. Energy dissipation is modeled using viscous damping, while the interaction with the workpiece is represented as a localized external force.

Under these assumptions, the governing equation for the tensioned blade is:

$$\rho A \frac{\partial^2 w(x,t)}{\partial t^2} + c \frac{\partial w(x,t)}{\partial t} - T \frac{\partial^2 w(x,t)}{\partial x^2} = q(x,t) \qquad (1)$$

where ρA is the mass per unit length, c is the damping coefficient, and T is the axial tension in the blade. The term $q(x,t)$ represents the external force per unit length acting on the blade.

The blade operates in a tension-dominated regime, where the contribution of bending stiffness is negligible. This assumption can be justified by the nondimensional parameter:

$$\eta = \frac{EI}{TL^2} \quad (2)$$

where E is Young's modulus and I is the second moment of area. For $\eta \ll 1$, the system behaves as a tensioned string, and bending effects can be neglected [3].

Using the representative blade dimensions adopted in the simulations, with a width of approximately 0.10 m, a thickness of approximately 1.0×10^{-3} m, Young's modulus $E \approx 2.0 \times 10^{11}$ Pa, axial tension $T = 2.0 \times 10^4$ N, and guide spacing $L = 0.31$ m, the weak-axis second moment of area is approximately $I = \frac{bh^3}{12} \approx 8.3 \times 10^{-12}$ m^4, which gives $\eta = \frac{EI}{TL^2} \approx 8.7 \times 10^{-4}$. Since $\eta \ll 1$, the tension-induced restoring effect is dominant for the investigated configuration. Nevertheless, bending stiffness may become relevant for lower blade tension, shorter guide spacing, thicker blades, or local deformation near the guides and cutting zone.

The tensioned-string approximation should be regarded as a reduced first-order description of the active blade span. Within this formulation, bending stiffness, torsional vibration, local tooth geometry, blade–guide compliance, wheel–blade interaction, and three-dimensional deformation near the cutting zone are not explicitly included. These effects may become important in a more detailed predictive model, particularly near the guides or under conditions involving large-amplitude motion, local contact loss, or significant torsional response.

The present one-dimensional model is therefore intended primarily to isolate the influence of localized cutting and frictional loading on the lateral motion of a highly tensioned blade. The guide-bounded formulation captures the dominant transverse response of the active span while retaining a transparent and computationally efficient structure suitable for parametric analysis.

2.2. Localized cutting and frictional loading

Fig. 1 illustrates the active blade span considered in the model. The blade is laterally constrained by two guides separated by the distance L, while the cutting action is applied at the position x_0. The lateral displacement is denoted by $w(x,t)$, and the blade is subjected to the axial tension T. The localized transverse loading consists of the cutting-force component $F_c(t)$ and the effective friction force $F_f = \mu F_N$, where F_N is the representative normal contact force.

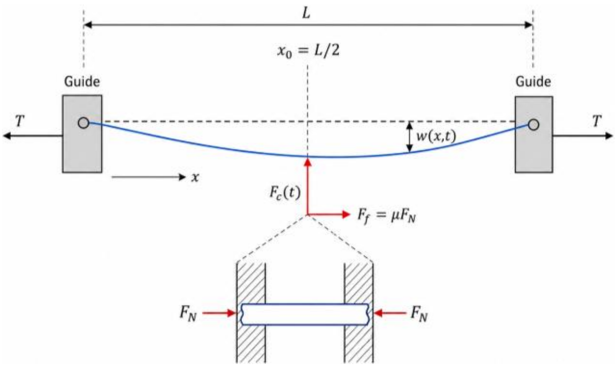

Fig. 1. Schematic representation of the guide-bounded active blade span and the applied forces.

The cutting force is applied locally at position x_0, and is introduced using a Dirac delta function:

$$q(x,t) = F(t)\,\delta(x - x_0) \quad (3)$$

In the absence of friction, the cutting force is modeled as a nonlinear function of feed speed with an additional time-dependent perturbation:

$$F_c(t) = K\left(\frac{v_f}{v_s}\right)^n + \Delta F \sin(\omega t) \quad (4)$$

where K is the cutting-force coefficient, v_f is the feed speed, v_s is the blade speed, n is an empirical exponent describing the dependence of force on feed speed, and ΔF and ω represent the amplitude and frequency of dynamic perturbations, respectively [8,16].

The harmonic perturbation term $\Delta F \sin(\omega t)$ represents the dynamic component of the cutting force. In actual band sawing, the force acting on the blade is not perfectly steady even when the feed speed is constant. Periodic and quasi-periodic fluctuations may arise from repeated tooth engagement, intermittent blade–workpiece contact, local variations in chip formation, knots or density variations in the wood, and machine-induced vibrations. The sinusoidal term is therefore not intended to reproduce the full tooth-level force history, but to provide a simplified representation of the dominant dynamic excitation acting at the cutting zone.

Band sawing is inherently a tribological process involving frictional interaction between the blade and the workpiece. In addition to the cutting force associated with material removal, friction arises from contact between the lateral surfaces of the blade and the workpiece, contributing to the total force acting on the blade [4,5].

The total force is therefore expressed as the sum of cutting and frictional contributions:

$$F(t) = F_c(t) + F_f(t) \tag{5}$$

The frictional force is modeled using a Coulomb-type formulation:

$$F_f(t) = \mu F_N \tag{6}$$

where μ is the coefficient of friction and F_N is the normal contact force acting on the lateral blade surface.

The Coulomb-type formulation adopted in the present study should be interpreted as an effective model of the lateral frictional load rather than as a complete description of the blade–wood contact. The normal contact force F_N is represented by a constant mean value associated with the lateral pressure exerted by the workpiece on the blade surfaces. This pressure arises from elastic–plastic recovery of the wood and depends on wood species, moisture content, kerf geometry, cutting depth, blade inclination, and local deformation [4,5].

In actual cutting conditions, both F_N and the coefficient of friction μ may vary in space and time. They may also depend on contact pressure, wood anisotropy, surface roughness, temperature, lubrication conditions, and tool wear [4,5]. These effects are not explicitly included in the present formulation. The use of constant values of F_N and μ is therefore intended to isolate the influence of the frictional contribution in a controlled parametric analysis. The adopted model provides a transparent first-order representation of friction-induced loading, while more detailed prediction for a specific industrial machine would require a state-dependent friction law and experimentally calibrated contact parameters.

Substituting Eq. (6) into Eq. (5) and using the expression (4) for the cutting force, the total force becomes:

$$F(t) = K\left(\frac{v_f}{v_s}\right)^n + \Delta F \sin(\omega t) + \mu F_N \tag{7}$$

The governing equation thus takes the form:

$$\rho A \frac{\partial^2 w}{\partial t^2} + c\frac{\partial w}{\partial t} - T\frac{\partial^2 w}{\partial x^2} = [K(\frac{v_f}{v_s})^n + \Delta F \sin(\omega t) + \mu F_N]\,\delta(x - x_0) \tag{8}$$

This formulation enables direct comparison between the frictionless case ($\mu = 0$) and frictional cases ($\mu > 0$), allowing systematic investigation of the influence of the coefficient of friction on blade dynamics. For $\mu = 0$ the model reduces identically to the baseline cutting-force-only model.

The analysis is restricted to the active free span of the blade located between two lateral guides. The guides constrain the transverse motion of the blade at the ends of the considered domain, while the cutting force acts within this span. Accordingly, the spatial coordinate is defined over $0 \leq x \leq L$, where L denotes the effective distance between the blade guides.

The transverse displacement at both guide locations is assumed to vanish, leading to the fixed-end boundary conditions

$$w(0,t) = 0, w(L,t) = 0. \tag{9}$$

These boundary conditions represent the lateral restraint imposed by properly adjusted blade guides. The guide-bounded formulation prevents rigid-body lateral motion of the entire blade loop and enables the model to describe the local dynamic response of the blade segment directly involved in cutting. Inadequate guide support or an excessively large guide spacing would reduce the lateral restraint and may lead to substantially larger blade deflections.

The initial conditions are defined for an undeformed blade at rest:

$$w(x,0) = 0, \frac{\partial w(x,0)}{\partial t} = 0 \tag{10}$$

The governing equation is solved numerically using the finite difference method [17]. The spatial domain $[0, L]$ is discretized as:

$$x_i = i\Delta x, i = 1,2,\dots,N_x \tag{11}$$

and time is discretized as:

$$t^n = n\Delta t, n = 0,1,\dots,N_t \tag{12}$$

with $\Delta x = L/(N_x - 1)$ and Δt chosen to satisfy the stability condition.

The second spatial derivative is approximated by the standard central difference:

$$\frac{\partial^2 w}{\partial x^2}\Big|_{(x_i,t^n)} \approx \frac{w_{i+1}^n - 2w_i^n + w_{i-1}^n}{\Delta x^2} \tag{13}$$

The second time derivative is also discretized centrally:

$$\frac{\partial^2 w}{\partial t^2}\Big|_{(x_i,t^n)} \approx \frac{w_i^{n+1} - 2w_i^n + w_i^{n-1}}{\Delta t^2} \tag{14}$$

The first time derivative associated with viscous damping is approximated by a centred difference,

$$\frac{\partial w}{\partial t}\Big|_{(x_i,t^n)} \approx \frac{w_i^{n+1} - w_i^n}{\Delta t} \tag{15}$$

Substituting these approximations into Eq. (8) yields the discrete equation:

$$\rho A \frac{w_i^{n+1} - 2w_i^n + w_i^{n-1}}{\Delta t^2} + c\frac{w_i^{n+1} - w_i^n}{\Delta t} - T\frac{w_{i+1}^n - 2w_i^n + w_{i-1}^n}{\Delta x^2} = q_i^n \tag{16}$$

where q_i^n is the discrete approximation of the external force per unit length at node i and time step n. The force is applied only at the node i_0 closest to the cutting position, using the consistent approximation:

$$q_i^n = \begin{cases} \frac{F(t^n)}{\Delta x}, & i = i_0 \\ 0, & i \neq i_0 \end{cases} \tag{17}$$

This guarantees that the total force applied on the blade equals $F(t^n)$.

Solving Eq. (16) for w_i^{n+1} yields the explicit time-marching formula:

$$w_i^{n+1} = \{(2\rho A + c\Delta t)\, w_i^n \;-\; \rho A\, w_i^{n-1} \;+\; T\frac{\Delta t^2}{\Delta x^2}(w_{i+1}^n - 2w_i^n + w_{i-1}^n) \;+\; \Delta t^2\, q_i^n\}/\{\rho A + c\Delta t\} \tag{18}$$

The stability of this explicit scheme is controlled by the Courant–Friedrichs–Lewy condition for the undamped wave part:

$$\Delta t \le \frac{\Delta x}{\sqrt{T/(\rho A)}} \tag{19}$$

In all simulations, a time step of $\Delta t = 0.5\,\Delta x/\sqrt{T/(\rho A)}$ is used, which guarantees stable integration while keeping numerical dispersion low.

The simulation starts from the initial conditions (10). Using a Taylor expansion and the discrete equations, the first two time levels are initialised as:

$$w_i^0 = 0, w_i^1 = \frac{\Delta t^2}{2}\,\frac{q_i^0}{\rho A} \tag{20}$$

which correspond to a blade initially at rest that begins to move under the instantaneous applied force.

The explicit update formula is applied only to the interior nodes $i = 2, \ldots, N_x - 1$. The transverse displacement at the two boundary nodes is prescribed directly by the fixed-end conditions, $w_1^j = 0, w_{N_x}^j = 0$, for all time levels j. Accordingly, the central - difference approximation is evaluated at each interior node using the neighbouring values w_{i-1}^j and w_{i+1}^j, while the guide locations remain fixed throughout the simulation.

The first two time levels are initialized consistently with the undeformed and stationary initial state. At the boundary nodes, $w_1^1 = w_{N_x}^1 = 0$, $w_1^2 = w_{N_x}^2 = 0$, whereas the second time level at the interior nodes is obtained from Eq. (20).

The numerical scheme described above provides an efficient and physically consistent framework for simulating the distributed dynamic response of the band saw blade. By incorporating the frictional term directly through μF_N in the total force (7), the model enables a transparent investigation of how the coefficient of friction affects the lateral vibration of the blade. The specific parameter values used in the simulations, including the chosen constant normal force F_N, are reported and physically justified in the following section.

3. RESULTS

3.1 Numerical solution and model parameters

The numerical solution of the governing equation is carried out using the finite difference scheme derived in Section 2. The explicit time-stepping formula (Eq. 18) is applied on a uniform spatial grid with $N_x = 201$ nodes, giving a spatial step $\Delta x = L/(N_x - 1)$. The time step is set to

$$\Delta t = 0.5\,\frac{\Delta x}{\sqrt{T/(\rho A)}} \tag{21}$$

which satisfies the stability condition (19) and provides accurate temporal resolution. The total simulated time is $t_{\max} = 0.1$ s, long enough to capture both the initial transient and the steady oscillatory regime.

The physical parameters of the blade correspond to a typical steel band saw used in primary wood processing. The mass per unit length is taken as $\rho A = 0.8$ kg/m, consistent with a blade thickness of about 1 mm and width around 10 cm. The axial tension is set to $T = 2 \times 10^4$ N, a value within the industrial range [2,3]. The effective damping coefficient, accounting for internal material dissipation, aerodynamic effects, and cutting-zone interactions, is chosen as $c = 50$ kg/(m s) [1].

The analysed domain represents the active free span of the blade between two lateral guides rather than the entire closed blade loop. The effective guide spacing is taken as $L = 0.31$ m, corresponding to the approximately 310 mm spacing between the guides used in the experimental band-saw configuration reported by Tandler and Möhring [18]. The cutting position is placed at the midpoint of the guided span, $x_0 = \frac{L}{2} = 0.155$ m. This configuration enables a literature-based comparison between the predicted displacement at the cutting zone and experimentally reported lateral blade deflection within a guide-bounded span.

The cutting process is defined by the blade speed $v_s = 30$ m/s and a feed speed that is varied in the interval $v_f = 0.01 - 0.1$ m/s. This range reflects typical industrial conditions for cross-sawing of wood [8]. The cutting force coefficient is $K = 500$ N and the exponent $n = 1$, which corresponds to a linear dependence of the cutting force on the feed per tooth in the first approximation [16]. The oscillatory perturbation that mimics tooth impacts, material inhomogeneities and intermittent contact has an amplitude $\Delta F = 50$ N and a frequency $\omega = 200$ rad/s.

The adopted parameter values should be interpreted as representative effective values suitable for a first-order parametric analysis of band saw blade dynamics. The blade mass per unit length, axial tension, blade speed, guide spacing, and feed-speed interval correspond to realistic operating conditions for industrial band sawing. In contrast, the damping coefficient, cutting-force coefficient, perturbation amplitude, and normal contact force should be regarded as effective parameters that combine several physical mechanisms which are not modelled separately in the present formulation.

The damping coefficient accounts for internal material dissipation, aerodynamic losses, energy transfer through the blade guides, and dissipation in the cutting zone. The cutting-force coefficient provides an empirical relation between the feed conditions and the mean force associated with material removal. The harmonic perturbation amplitude represents periodic and quasi-periodic force variations caused by repeated tooth engagement, intermittent cutting, local variations in chip formation, and material inhomogeneity. The normal force F_N represents an effective average contact load acting on the lateral blade surfaces. Therefore, the adopted values are not intended to reproduce one specific machine in every detail, but to provide a physically reasonable basis for analysing the sensitivity of lateral blade motion to feed conditions and friction.

The tribological contribution is introduced through the coefficient of friction μ, which is varied from 0 to 0.6. This range covers the dry sliding conditions of wood–steel contacts reported in recent experimental studies [4,5]. The key novel element of the present model is the treatment of the normal contact force F_N that appears in the Coulomb friction term $F_f = \mu F_N$. Instead of tying F_N artificially to the feed speed, we estimate it from the lateral pressure that the workpiece exerts on the blade sides. During sawing, the wood undergoes elastic–plastic springback, generating a nearly constant lateral pressure on the blade. For a representative contact height of 10 mmand a contact length of 0.10 m, the corresponding nominal contact area is 1.0×10^{-3} m^2. An average lateral contact pressure of 0.10 MPa, within the range of wood–steel contact pressures considered in the literature [4], then yields a normal force of approximately 100 N on one side of the blade. Since both sides of the blade are in contact with the kerf walls, the total normal force is taken as

$$F_N = 200 \text{ N} \tag{22}$$

This value is kept constant throughout the parametric study, ensuring that the friction force is simply proportional to μ. The sensitivity of the results to this choice is discussed later.

With the cutting force given by Eq. (4) and the friction force by Eq. (6), the total force applied at the cutting point becomes

$$F(t) = K\left(\frac{v_f}{v_s}\right)^n + \Delta F \sin(\omega t) + \mu F_N \tag{23}$$

The external load is distributed onto the numerical grid via the discrete delta function (17). The cutting position is fixed at the midpoint of the active blade span, $x_0 = L/2 = 0.155$ m.

All simulations start from an undeformed blade at rest, i.e. $w(x,0) = 0$ and $\partial w/\partial t(x,0) = 0$. The first two time levels are initialised according to Eq. (20).

In the following section, the baseline response of the blade is first analysed for the frictionless case $\mu = 0$, which serves as a reference. The effect of friction is then investigated in Section 3.3 by varying μ while keeping all other parameters fixed.

3.2 Baseline blade response without friction

In order to establish a reference case for comparison with the frictional simulations, the dynamic response of the band saw blade is first analysed for the baseline case without friction. Under this condition, the tribological model reduces to the cutting-force-only formulation, comprising the feed-dependent mean component and the harmonic dynamic perturbation. The results presented in this section therefore represent the reference blade response in the absence of the additional frictional load.

The primary quantity of interest is the lateral displacement of the blade at the cutting position, $w(x_0, t)$, which directly governs the deviation of the blade at the location where material separation takes place. The time evolution of this displacement for three different feed speeds is shown in Fig. 2.

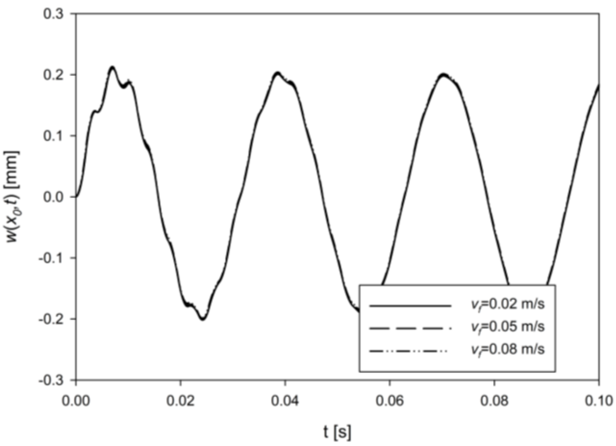

Fig. 2. Time history of lateral displacement at the cutting position ($x_0 = 1.0$ m) for different feed speeds in the baseline case without friction ($\mu = 0$).

As can be seen from Fig. 2, the system response is characterised by a short initial transient, after which the oscillations settle into a bounded quasi-periodic regime. Immediately after the onset of cutting, the blade is set into motion by the sudden application of the localised force. The transient growth is controlled by inertia and axial tension, while the subsequent steady oscillations are sustained by the time-dependent part of the excitation. The viscous damping prevents unbounded growth and forces the system to oscillate around a displaced equilibrium position.

The three response curves are almost indistinguishable over the considered feed-speed range. This behaviour follows directly from the adopted cutting-force model. The feed-dependent static component of the force varies only from approximately 0.33 N to 1.33 N, whereas the amplitude of the harmonic perturbation is 50 N. Consequently, the lateral vibration is governed primarily by the dynamic excitation, while the influence of feed speed on both the mean displacement and the oscillation amplitude remains very small.

The near-overlap of the curves should therefore not be interpreted as numerical insensitivity, but as a physical consequence of the relative magnitudes of the force components. Under the selected operating conditions, changes in feed speed produce only a minor modification of the blade response compared with the periodic excitation associated with tooth engagement, intermittent cutting, and material inhomogeneity.

From an engineering perspective, the near-overlap of the curves indicates that variations in feed speed within the investigated range do not substantially alter the lateral blade response under the adopted force parameters. Although feed speed affects the mean cutting-force component, its contribution remains small compared with the harmonic excitation. Consequently, the present baseline results do not indicate a pronounced deterioration of blade stability with increasing feed speed alone; instead, they identify dynamic force fluctuations as the dominant source of lateral motion in the frictionless case.

The spatial distribution of lateral displacement along the blade at the final simulation time ($t = 0.1$ s) is presented in Fig. 3.

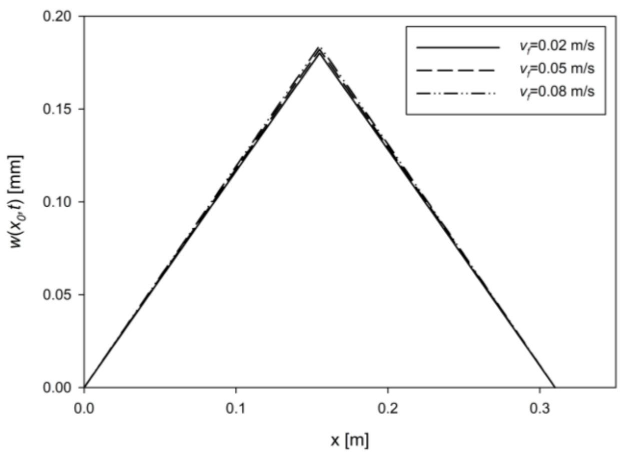

Fig. 3. Spatial distribution of lateral blade displacement at the end of the simulation for different feed speeds in the baseline case ($\mu = 0$).

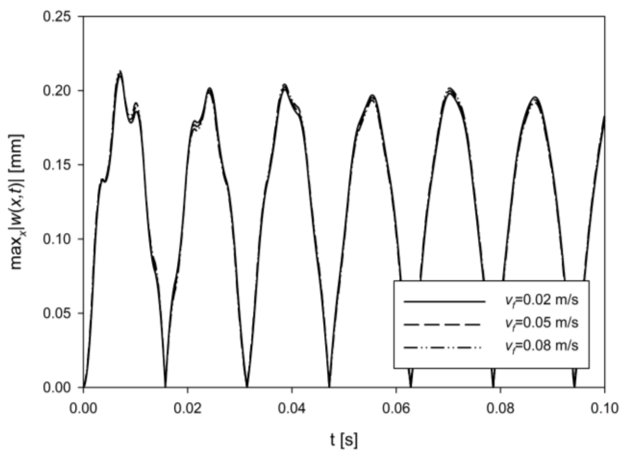

Fig. 4. Time evolution of the maximum absolute blade displacement for different feed speeds in the baseline case ($\mu = 0$).

The spatial profiles are symmetric about the cutting position and satisfy the prescribed zero-displacement conditions at the two blade guides. The largest displacement occurs at the midpoint of the free span, where the localized cutting force is applied, and decreases smoothly toward the guide locations. This profile reflects the redistribution of the concentrated transverse load through the axial tension of the blade.

As in the time histories shown in Fig. 2, the spatial profiles obtained for the three feed speeds almost completely overlap. The feed-dependent contribution to the applied force is too small relative to the harmonic perturbation to produce a clearly distinguishable change in the displacement profile. The blade shape is therefore controlled primarily by the guide-bounded geometry, the axial tension, and the localized dynamic excitation.

To capture the overall severity of the blade motion, the maximum absolute displacement taken over the whole spatial domain is plotted as a function of time in Fig. 4.

The time evolution of the maximum absolute displacement follows the same general pattern as the local response at the cutting position. After a short transient, the response remains bounded and oscillatory for all considered feed speeds. The corresponding curves are again almost indistinguishable, confirming that the feed-dependent part of the applied force has only a minor influence on the overall blade response under the selected conditions.

The baseline results therefore show that, within the investigated feed-speed range, the blade dynamics are controlled primarily by the harmonic perturbation rather than by the mean feed-dependent cutting force. The maximum absolute displacement changes only slightly with feed speed, because the corresponding static force contribution remains much smaller than the amplitude of the dynamic excitation. The frictionless case consequently provides a stable and well-defined reference for assessing the additional influence of friction in the following section.

Although the baseline case does not include frictional effects, it provides an essential lower-bound reference for the subsequent analysis. In real cutting conditions, friction at the blade–workpiece interface introduces an additional force component that may increase the excitation level [4,5]. The frictionless solution therefore serves as a physically consistent reference state for evaluating the relative influence of the tribological contribution introduced in the following section.

3.3 Influence of friction on blade dynamics

In this section, the influence of friction on the dynamic response of the band saw blade is investigated by introducing a non-zero coefficient of friction μ into the force model. The analysis is performed at the highest feed speed considered in the baseline simulations, $v_f = 0.08\,\mathrm{m/s}$, while all other mechanical and numerical parameters are kept unchanged. For the time-dependent and spatial-response analyses, the coefficient of friction is varied from $\mu = 0$ to 0.6 in increments of 0.2. Additional simulations at $\mu = 0.1$, 0.3, and 0.5 are included in the quantitative dependence of the maximum displacement on the coefficient of friction. The complete investigated range is consistent with dry wood–steel sliding conditions reported in the literature [4,5].

To avoid ambiguity, two related response measures are used in the following analysis. The local displacement at the cutting position is denoted by $w(x_0, t)$, whereas the maximum absolute displacement over the active blade span is defined as $w_{\max}(t) = \max_{0 \le x \le L} | w(x,t) |$. The former describes the motion directly at the cutting zone, while the latter represents the largest instantaneous deflection anywhere between the two guides. Figs. 5 and 6 show the local and spatial responses, respectively, whereas Figs. 7 and 8 are based on the maximum absolute displacement $w_{\max}$.

The time evolution of the blade displacement at the cutting position for different values of the friction coefficient is presented in Fig. 5.

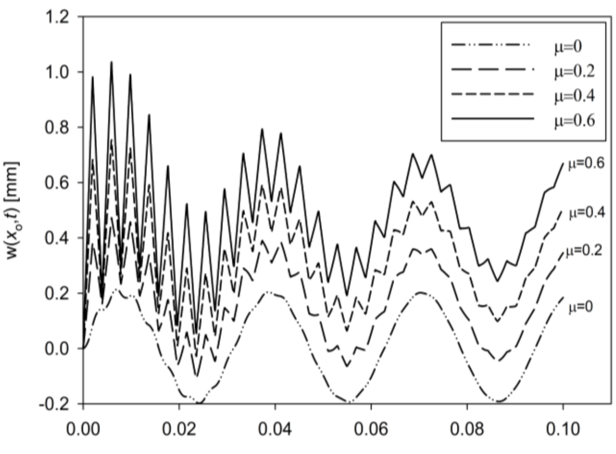

Fig. 5. Time history of lateral displacement at the cutting position ($x_0 = 1.0$ m) for different values of the coefficient of friction ($v_f = 0.08$ m/s).

As shown in Fig. 5, increasing the coefficient of friction produces a clear and systematic increase in the lateral displacement at the cutting position. The overall character of the response remains unchanged: after a short transient, the blade exhibits bounded oscillations for all considered values of μ. However, the mean displacement level and the oscillation amplitude both increase with friction.

For the reference frictionless case, the maximum displacement remains of the order of 0.2 mm. As the coefficient of friction increases, the peak displacement rises progressively and reaches approximately 1.0 mmfor $\mu = 0.6$. Thus, under the adopted guide-bounded configuration, friction increases the maximum lateral response by approximately a factor of five relative to the baseline case.

This behaviour follows directly from the additional Coulomb-type contribution $F_f = \mu F_N$. With the normal contact force fixed at $F_N = 200$ N, the friction force increases from 0 to 120 N over the considered range of μ. The resulting increase in the total transverse load explains the monotonic amplification of blade displacement. At the same time, the fixed guide spacing limits the response and prevents the excessive lateral motion that would occur in a weakly constrained or excessively long free span.

The spatial distribution of blade displacement at the final simulation time ($t = 0.1$ s) is shown in Fig. 6.

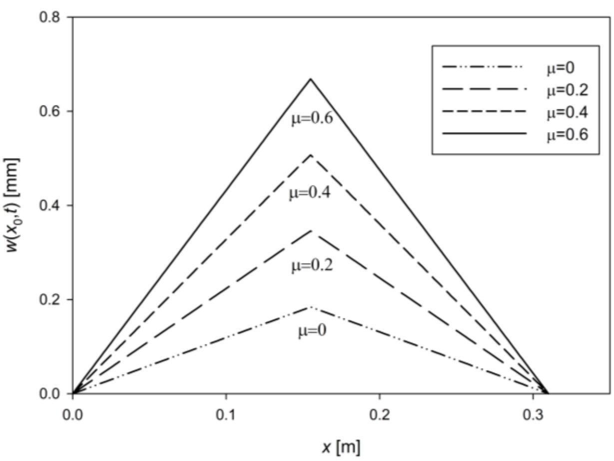

Fig. 6. Spatial distribution of lateral blade displacement at the end of the simulation for different values of the coefficient of friction ($v_f = 0.08$ m/s).

The spatial profiles remain symmetric about the cutting position and satisfy the zero-displacement conditions at the guide locations. For all values of μ, the largest displacement occurs near the midpoint of the free span, where the localized force is applied, while the response decreases smoothly toward the two guides.

Increasing the coefficient of friction preserves the overall shape of the displacement profile but increases its amplitude throughout the active blade span. For $\mu = 0.6$, the displacement at the cutting position reaches approximately 1.0 mm, compared with about 0.2 mm in the frictionless case. This confirms that the local frictional contribution affects the global deformation of the guide-bounded blade segment through the redistribution of the applied load by axial tension.

The persistence of the same spatial shape for different values of μ reflects the linear structure of the governing equation and the fact that only the magnitude of the localized excitation is changed, while the blade properties, guide spacing, and cutting position remain fixed.

The time evolution of the maximum absolute displacement along the entire blade is presented in Fig. 7.

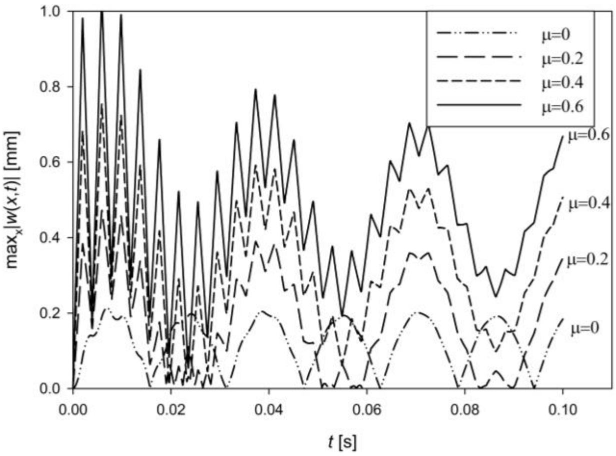

Fig. 7. Time evolution of the maximum absolute blade displacement for different values of the coefficient of friction ($v_f = 0.08$ m/s).

Fig. 7 confirms that the maximum absolute displacement increases systematically with the coefficient of friction while remaining bounded for all considered cases. After the initial transient, the response approaches a stable oscillatory regime, indicating that the guide-bounded blade segment remains dynamically stable within the investigated parameter range.

The maximum absolute displacement increases from approximately 0.21 mm for $\mu = 0$ to about 1.04 mm for $\mu = 0.6$. The corresponding increase is therefore close to a factor of five. This result is consistent with the time histories at the cutting position and with the spatial profiles shown in Fig.s. 5 and 6.

The regular variation of the response with μ reflects the additive form of the friction force in the model. Because the blade geometry, guide spacing, axial tension, damping, and cutting conditions remain unchanged, the observed differences arise primarily from the increasing magnitude of the term μF_N.

To provide a quantitative summary of the influence of friction, the maximum absolute blade displacement attained during the simulated time interval is plotted as a function of the coefficient of friction in Fig. 8.

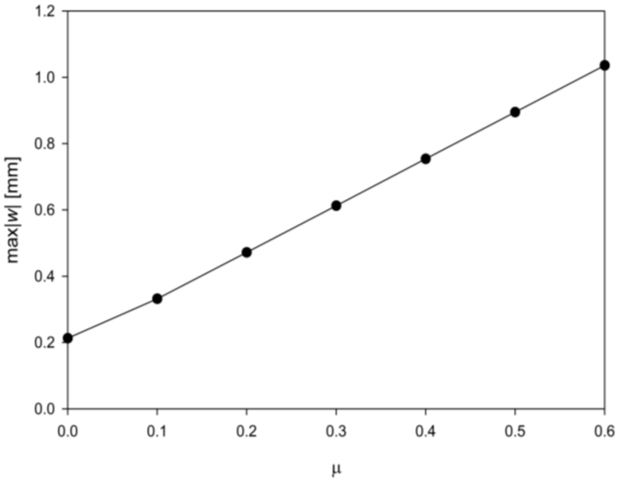

Fig. 8. Dependence of the maximum lateral blade displacement on the coefficient of friction μ for $v_f = 0.08$ m/s.

To assess the sensitivity of the predicted response to the assumed normal contact force, additional simulations were performed for $F_N = 100, 150,$ and 200 N, while keeping $\mu = 0.6$ and all other parameters unchanged. The corresponding maximum lateral displacements were 0.613, 0.825, and 1.036 mm, respectively.

The approximately linear increase of the maximum displacement with F_N is consistent with the adopted friction law $F_f = \mu F_N$. This sensitivity analysis confirms that the absolute displacement values depend directly on the assumed effective normal contact force, whereas the qualitative conclusion remains unchanged: increasing the frictional load produces a systematic amplification of the lateral blade response. The value $F_N = 200$ N is retained as the reference case because it follows from the estimated lateral contact pressure acting on both sides of the blade.

The dependence of the maximum lateral displacement on the coefficient of friction is approximately linear over the investigated range. The maximum displacement increases from 0.213 mm for $\mu = 0$ to 1.036 mm for $\mu = 0.6$. The intermediate values are 0.332, 0.472, 0.613, 0.754, and 0.895 mm for $\mu = 0.1, 0.2, 0.3, 0.4$, and 0.5, respectively.

This nearly linear trend is expected from the adopted force model, in which the friction contribution is given by $F_f = \mu F_N$ with constant F_N. Therefore, the result should not be interpreted as an independently emerging nonlinear tribological law, but as a direct quantitative consequence of the additive Coulomb-type loading within the linear blade model. Its practical significance lies in showing how strongly the predicted lateral response changes across a physically relevant range of friction coefficients.

The predicted displacement magnitude was compared with the experimental results reported by Tandler and Möhring [18] for a band-saw configuration with an approximately 0.31 m guide spacing. For the highest considered friction coefficient, $\mu = 0.6$, the present model predicts a maximum lateral displacement of approximately 1.04 mm. This value is practically in the range of the experimentally estimated maximum displacement of approximately 0.9–1.0 mm within the guide-bounded span. The close agreement in magnitude supports the physical plausibility of the revised model configuration, although it should not be interpreted as a complete validation because the exact blade geometry, cutting conditions, material properties, and contact parameters are not identical in the two cases.

The comparison also demonstrates the importance of blade guides in controlling lateral motion. Properly positioned guides restrict the active free span and prevent excessive lateral displacement. Conversely, an increased guide spacing or insufficient lateral restraint may substantially amplify blade deflection and adversely affect cutting accuracy, surface quality, and dimensional tolerances.

From an engineering perspective, the predicted increase in lateral displacement has direct implications for sawing performance. Larger deflections at the cutting zone may increase kerf deviation, reduce dimensional accuracy, and promote surface waviness, particularly in narrow-kerf cutting where small changes in blade position can visibly affect the sawn surface. Increased friction may also raise local heat generation and accelerate tool wear, which can further modify the contact conditions and intensify the blade response [4,5,11]. The results therefore indicate that blade surface condition, tool wear, wood moisture content, guide adjustment, coatings, and lubrication may influence both tribological behaviour and cutting stability. Nevertheless, the present formulation remains a reduced parametric model based on an effective Coulomb-type lateral load; machine-specific quantitative prediction would require experimentally calibrated contact parameters and more detailed blade–guide mechanics.

4. CONCLUSION

In this study, a distributed-parameter model of the lateral dynamic response of a band saw blade was developed by combining a tension-dominated mechanical description with an effective Coulomb-type friction load. The analysed domain represents the active blade span between two lateral guides, while the cutting and frictional forces act locally at the midpoint of the span.

The guide-bounded formulation produces a localized and physically constrained blade response. For the frictionless case, the lateral displacement is governed primarily by the harmonic component of the cutting force, whereas the influence of feed speed remains small over the investigated range. The calculated response remains bounded and oscillatory after a short initial transient.

The inclusion of friction produces a systematic increase in lateral blade displacement. For the adopted normal contact force $F_N = 200$ N, the maximum displacement increases from 0.213 mmfor $\mu = 0$ to 1.036 mm for $\mu = 0.6$, corresponding to an increase by approximately a factor of five. The dependence is nearly linear because the frictional contribution enters the model through the additive term $F_f = \mu F_N$.

The sensitivity analysis performed for $F_N = 100$, 150, and 200 N confirms that the predicted displacement magnitude depends directly on the assumed effective normal contact force. Nevertheless, the qualitative conclusion remains unchanged: stronger frictional loading produces a larger lateral response while the blade remains dynamically bounded within the investigated parameter range.

For a guide spacing of $L = 0.31$ m, the predicted maximum displacement of approximately 1.04 mm is in the range of the experimentally estimated displacement reported for a guide-bounded band-saw configuration reported in the literature. This agreement supports the physical plausibility of the model, although it does not constitute a complete machine-specific validation because the exact blade geometry, cutting conditions, material properties, and contact parameters differ.

The results also demonstrate the importance of blade guides. By restricting the active free span, the guides limit lateral displacement and help maintain cutting accuracy.

The present model should be regarded as a reduced parametric description. It neglects bending stiffness, torsional motion, guide compliance, wheel–blade interaction, state-dependent friction, local contact-pressure variations, temperature effects, and wear evolution. Future work should include experimentally calibrated contact parameters, more detailed guide and blade mechanics, and direct validation under controlled cutting conditions.

Acknowledgement

The research was under grant from Serbian Ministry of Science, Technological Development and Innovations (Agreement No. 451-03-34/2026-03/ 200122).

REFERENCES

[1] S. P. Timoshenko and D. H. Young, *Vibration Problems in Engineering*, 3rd ed. New York, NY, USA: D. Van Nostrand, 1955.

[2] A. G. Ulsoy and C. D. Mote, Jr., "Band saw vibration and stability," *The Shock and Vibration Digest*, vol. 10, no. 11, pp. 3–15, Nov. 1978, doi: 10.1177/058310247801001101.

[3] A. G. Ulsoy and C. D. Mote, Jr., "Analysis of bandsaw vibration," *Wood Science*, vol. 13, no. 1, pp. 1–10, Jul. 1980.

[4] M. Dorn, K. Habrová, R. Koubek, and E. Serrano, "Determination of coefficients of friction for laminated veneer lumber on steel under high pressure loads," *Friction*, vol. 9, pp. 367–379, 2021, doi: 10.1007/s40544-020-0377-0.

[5] Y. Zheng, A. Cabboi, and J.-W. van de Kuilen, "Identification of the coefficient of sliding friction from an apparent non-Coulomb behavior between wood and steel," *Tribology International*, vol. 200, Art. no. 110193, 2024, doi: 10.1016/j.triboint.2024.110193.

[6] P. Iskra and R. E. Hernández, "The influence of cutting parameters on the surface quality of routed paper birch and surface roughness prediction modeling," *Wood and Fiber Science*, vol. 41, no. 1, pp. 28–37, 2009.

[7] K. A. Orlowski, T. Ochrymiuk, and A. Atkins, "An innovative approach to the forecasting of energetic effects while wood sawing," *Drvna industrija*, vol. 65, no. 4, pp. 273–281, 2014, doi: 10.5552/drind.2014.1341.

[8] J. Krilek, J. Melicherčík, T. Kuvik, J. Kováč, A. Gendek, M. Aniszewska, and J. Mareček, "Analysis of cutting forces in cross-sawing of wood: A study of sintered carbide and high-speed steel blades," *Forests*, vol. 14, no. 7, Art. no. 1395, 2023, doi: 10.3390/f14071395.

[9] K. A. Orlowski, Y. Huang, D. Chuchala, D. Buck, D. Stenka, M. Svensson, and M. Fredriksson, "Cutting forces for clear and knotty pine wood," in *Proceedings of the 25th International Wood Machining Seminar*, G. S. Schajer, Ed., Nagoya, Japan, Oct. 4–7, 2023.

[10] V. Meulenberg, M. Ekevad, and M. Svensson, "Minor cutting edge angles of sawing teeth: Effect on cutting forces in wood," *European Journal of Wood and Wood Products*, vol. 80, pp. 1165–1173, 2022, doi: 10.1007/s00107-022-01833-3.

[11] M. Torkghashghaei, W. Shaffer, B. Ugulino, R. Georges, R. E. Hernández, and C. Blais, "Improvement of the wear resistance of circular saws used in the first transformation of wood through the utilization of variable engineered micro-geometry performed on PVD-coated WC-Co tips," *Applied Sciences*, vol. 12, no. 23, Art. no. 12213, 2022, doi: 10.3390/app122312213.

[12] Y. Altintas, *Manufacturing Automation: Metal Cutting Mechanics, Machine Tool Vibrations, and CNC Design*, 2nd ed. Cambridge, U.K.: Cambridge University Press, 2012.

[13] E. Budak, "Analytical models for high performance milling. Part I: Cutting forces, structural deformations and tolerance integrity," *International Journal of Machine Tools and Manufacture*, vol. 46, no. 12–13, pp. 1478–1488, 2006, doi: 10.1016/j.ijmachtools.2005.09.009.

[14] P. Olejnik and Y. D. Desta, "Friction-induced interactions: acoustic emissions, vibrations, and wear – a multiscale review," *Nonlinear Dynamics*, vol. 113, pp. 24101–24140, 2025, doi: 10.1007/s11071-025-11397-5.

[15] A. Ahsan, K. Kenney, J. Kröger, and S. Böhm, "Hydrostatic bandsaw blade guides for natural stone-cutting applications," *Journal of Manufacturing and Materials Processing*, vol. 4, no. 1, Art. no. 20, 2020, doi: 10.3390/jmmp4010020.

[16] T. Atkins, *The Science and Engineering of Cutting: The Mechanics and Processes of Separating, Scratching and Puncturing Biomaterials, Metals and Non-metals*. Oxford, U.K.: Butterworth-Heinemann, 2009.

[17] G. D. Smith, *Numerical Solution of Partial Differential Equations: Finite Difference Methods*. Oxford, U.K.: Oxford University Press, 1985.

[18] T. Tandler and H.-C. Möhring, "Active runout compensation using the guide elements on metal band saws for a longer tool life and reduced material loss," *Production Engineering*, vol. 19, pp. 89–99, 2025, doi: 10.1007/s11740-024-01296-w.